Relaxed Alternating Direction Method of Multipliers for Hedging Communication Packet Loss in Integrated Electrical and Heating System

Xinyu Liang, Zhigang Li, *Member*, *IEEE*, Wenjing Huang, Q. H. Wu, *Fellow*, *IEEE*, and Haibo Zhang

***Abstract*—Integrated electrical and heating systems (IEHSs) are promising for increasing the flexibility of power systems by exploiting the heat energy storage of pipelines. With the recent development of advanced communication technology, distributed optimization is employed in the coordination of IEHSs to meet the practical requirement of information privacy between different system operators. Existing studies on distributed optimization algorithms for IEHSs have seldom addressed packet loss during the process of information exchange. In this paper, a distributed paradigm is proposed for coordinating the operation of an IEHS considering communication packet loss. The relaxed alternating direction method of multipliers (R-ADMM) is derived by applying Peaceman-Rachford splitting to the Lagrangian dual of the primal problem. The proposed method is tested using several test systems in a lossy communication and transmission environment. Simulation results indicate the effectiveness and robustness of the proposed R-ADMM algorithm.**

***Index Terms*—Alternating direction method of multipliers (ADMM), communication failure, distributed optimization, integrated energy systems, packet loss.**

NOMENCLATURE

A. Indices and Sets

Ω^{EPS}	Feasible region of electrical power system (EPS)
Ω_j^{DHS}	Feasible region of district heating system (DHS) j
$\mathcal{T}$	Index set of scheduling periods
A^{DHS}	Index set of areas in DHS
I^{EB}	Index set of electric boilers (EBs)
I^{HES}	Index set of heat exchanger stations
I^{HS}	Index set of heat sources
I^{HST}	Index set of heat storage tanks (HSTs)
I^{node}	Index set of nodes in the heating network
I^{pipe}	Index set of pipelines in the heating network
k	Index set of number of iterations
Nd_v^{HES}	Index set of nodes connected to heat exchanger station v
Nd_μ^{HS}	Index set of nodes connected to heat sources μ
S^{bus}	Index set of buses in EPS
S_j^{CHP}	Index set of combined heat and poewr (CHP) units connected to DHS j
S^{line}	Index set of lines in EPS
$S_i^{\mathrm{pipe}+}$	Index set of pipelines starting at node i
$S_i^{\mathrm{pipe}-}$	Index set of pipelines ending at node i
S^{TU}	Index set of thermal units
S^{wind}	Index set of wind farms

B. Input Parameters and Functions

η_h^{CHP}	Efficiency of CHP unit h
η_e^{EB}	Efficiency of EB e
$\underline{\tau}_{n,t}^{\mathrm{NS}}/\overline{\tau}_{n,t}^{\mathrm{NS}}$	Minimum/maximum temperatures at node n in the supply network
$\underline{\tau}_{m,t}^{\mathrm{NR}}/\overline{\tau}_{m,t}^{\mathrm{NR}}$	Minimum/maximum temperatures at node m in the return network
τ_t^{amb}	Ambient temperature in period t
δ_w	Penalty factor for curtailment of wind farm w
Δt	Time interval per period
λ_b	Heat transfer coefficient of pipeline b
$\phi_{b,t}/\gamma_{b,t}$	Number of time periods denoting time delays of pipeline b in period t

Manuscript received: March 16, 2020; accepted: August 18, 2020. Date of CrossCheck: August 18, 2020. Date of online publication: September 18, 2020.

This work was supported in part by the Key-Area Research and Development Program of Guangdong Province (No. 2020B010166004), the Guangdong Basic and Applied Basic Research Foundation (No. 2019A1515011408), the Talent Recruitment Project of Guangdong (No. 2017GC010467), and the State Key Laboratory of Alternate Electrical Power System with Renewable Energy Sources, North China Electric Power University (No. LAPS19011).

X. Liang, Z. Li (corresponding author), W. Huang, and Q. H. Wu are with the School of Electric Power Engineering, South China University of Technology, Guangzhou 510641, China (e-mail: ChelseaBiBi@hotmail.com; lizg16@scut.edu.cn; ephwj@mail.scut.edu.cn; wuqh@scut.edu.cn).

H. Zhang is with the State Key Laboratory of Alternate Electrical Power System with Renewable Energy Sources, North China Electric Power University, Beijing 102206, China (e-mail: zhb@ncepu.edu.cn).

DOI: 10.35833/MPCE.2020.000163

ρ^{ms} Density of water

ρ Penalty factor of the relaxed alternating direction method of multipliers (R-ADMM)

α Relaxed step size of the R-ADMM

$\varepsilon^{\mathrm{dual}}$ Feasibility tolerance for the dual residual

$\varepsilon^{\mathrm{pri}}$ Feasibility tolerance for the primal residual

$\boldsymbol{\lambda}_j$ Multipliers of the classical ADMM

A_b Cross-sectional area of pipeline b

$\boldsymbol{A}_j$ Coefficient of $\boldsymbol{x}^{\mathrm{EPS}}$ of the coupling constraint

$a_{p,h}$ The p^{th} cost coefficient of CHP unit h

$\boldsymbol{B}_j$ Coefficient of $\boldsymbol{y}_j^{\mathrm{DHS}}$ of the coupling constraint

$b_{q,g}$ The q^{th} cost coefficient of thermal unit g

c Specific heat capacity of water

$\boldsymbol{C}$ Coefficient of $\boldsymbol{\varphi}_{s,t}^{\mathrm{HST}}$

$\boldsymbol{d}$ Constant term of $\boldsymbol{\varphi}_{s,t}^{\mathrm{HST}}$

$D_{n,t}$ Electric loads at bus n in period t

$\underline{F}_l/\bar{F}_l$ Lower/upper flow limits on internal line l

$f(\cdot)$ Operation cost function of the EPS

$g_j(\cdot)$ Operation cost function of DHS j

$H_{v,t}^{\mathrm{HES}}$ Heat power output of heat exchanger station v in period t

$K_{b,t,k}$ The k^{th} coefficient of variables defining the outlet temperature of pipeline b in period t

$m_{v,t}^{\mathrm{HES}}$ Mass flow rate of heat exchanger station v in period t

$m_{\mu,t}^{\mathrm{HS}}$ Mass flow rate of heat sources μ in period t

$m_{b^+,t}^{\mathrm{PR}}$ Mass flow rate of pipeline b in the return network in period t

$m_{b^-,t}^{\mathrm{PS}}$ Mass flow rate of pipeline b in the supply network in period t

$\bar{p}_e^{\mathrm{EB}}$ Upper electricity consumption bound of EB e

$\underline{p}_g^{\mathrm{TU}}/\bar{p}_g^{\mathrm{TU}}$ Minimum/maximum generation output of thermal unit g

$\overline{p}_w^{\mathrm{wind}}$ Predicted available wind energy of wind farm w in period t

$p_j^{\mathrm{e}\to\mathrm{h}}$ Packet loss probability from an EPS to DHS j

$p_j^{\mathrm{h}\to\mathrm{e}}$ Packet loss probability from DHS j to an EPS

$RAMP_g^{\mathrm{down}}$ Downward ramping capability of thermal unit g

$RAMP_g^{\mathrm{up}}$ Upward ramping capability of thermal unit g

$RAMP_h^{\mathrm{down}}$ Downward ramping capability of CHP unit h

$RAMP_h^{\mathrm{up}}$ Upward ramping capability of CHP unit h

$R_{b,t}/S_{b,t}$ Coefficients of variables of pipeline b in period t associated with the historic mass flow

$SF_{l,n}$ Shift factor of bus n to line l

SR^{down} SR^{up} System-wide downward/upward spinning reserve capacity requirements

$\|\boldsymbol{r}(k)\|$ Primal residual in the k^{th} R-ADMM iteration

$\|\boldsymbol{s}(k)\|$ Dual residual in the k^{th} R-ADMM iteration

C. Decision Variables

$\tau_{i,t}^{\mathrm{NS}}/\tau_{i,t}^{\mathrm{NR}}$ Mixed temperatures at node i of the supply/return network in period t

$\tau_{b,t}^{\mathrm{PS,in}}/\tau_{b,t}^{\mathrm{PR,in}}$ Mass flow temperatures at the inlet of pipeline b in the supply/return network in period t

$\tau_{b,t}^{\mathrm{PS,out}}/\tau_{b,t}^{\mathrm{PR,out}}$ Mass flow temperatures considering temperature drop at the outlet of pipeline b in the supply/return network in period t

$\tau_{b,t}^{'\mathrm{PS,out}}/\tau_{b,t}^{'\mathrm{PR},out}$ Mass flow temperatures without temperature drop at the outlet of pipeline b in the supply/return network in period t

$\boldsymbol{\varphi}_{s,t}^{\mathrm{HST}}$ Vector of variables associated with HST s in period t

$L_j^{\mathrm{e}\to\mathrm{h}}(k)$ Independent binary random variables associated with packet loss during the k^{th} iteration from an EPS to DHS j

$L_j^{\mathrm{h}\to\mathrm{e}}(k)$ Independent binary random variables associated with packet loss during the k^{th} iteration from DHS j to an EPS

$p_{h,t}^{\mathrm{CHP}}$ Electricity production of CHP unit h in period t

$p_{e,t}^{\mathrm{EB}}$ Electricity consumption of EB e in period t

$p_{g,t}^{\mathrm{TU}}$ Electricity production of thermal unit g in period t

$p_{w,t}^{\mathrm{wind}}$ Electricity production of wind farm w in period t

$q_{h,t}^{\mathrm{CHP}}$ Heat production of CHP unit h in period t

$q_{e,t}^{\mathrm{EB}}$ Heat production of EB e in period t

$q_{s,t}^{\mathrm{HST}}$ Heat energy released from HST s in period t

$ru_{g,t}/rd_{g,t}$ Upward/downward spinning reserve capacities of thermal unit g in period t

$\boldsymbol{U}_j^{\mathrm{e}\to\mathrm{h}}(k)$ Delivered information from an EPS to DHS j in period t during the k^{th} iteration

$\boldsymbol{U}_j^{\mathrm{h}\to\mathrm{e}}(k)$ Delivered information from DHS j to an EPS in period t during the k^{th} iteration

$\boldsymbol{x}^{\mathrm{EPS}}$ Vector of all decision variables of the EPS

$\boldsymbol{y}_j^{\mathrm{DHS}}$ Vector of all decision variables of DHS j

$\boldsymbol{z}_j^{\mathrm{EPS}}(k)$ Auxiliary multipliers of an EPS associated with DHS j in period t during the k^{th} iteration

$\boldsymbol{z}_j^{\mathrm{DHS}}(k)$ Auxiliary multipliers of DHS j associated with an EPS in period t during the k^{th} iteration

I. Introduction

In recent years, integrated electrical and heating systems (IEHSs) have drawn extensive attention because of their potential to enhance the flexibility of accommodating more wind power. Equipped with combined heat and power (CHP) units, an IEHS can reuse the waste heat energy generated by power systems and supply heat and power loads simultaneously. The operation flexibility of CHP units is restricted in the heat-led operation mode [1]. During off-peak

hours in winter nights, the electricity demands are low while the heat loads are high. This situation leads to the poor utilization of wind power generation, which is seriously prominent in northern China [2]. Additional equipment investment can increase the utilization of wind power, such as heat pumps [3], electric boilers (EBs) [4], [5], and heat storage tanks (HSTs) [6]. Electric heater and heat storage device are integrated into power system to accommodate more extra wind power to improve economic benefit in [7]. Another way is to exploit pipelines or build energy storage in district heating systems (DHSs). Reference [8] proposes a dynamic temperature model of a DHS with time delay and heat loss. In [9], the thermal inertia of buildings is considered in the secondary heating network.

The solution methods for optimizing the IEHS can be classified into the metaheuristic algorithms and the mathematical programming techniques. The metaheuristic algorithms, such as the genetic algorithm [10], the particle swarm optimization [11], the group search optimization [12], and the differential evolution [13], have recently been improved to solve the IEHS problems. However, the computation time is long and premature convergence easily plunges into local minima for these algorithms. The electrical power systems (EPSs) and DHSs are controlled by different independent system operators (ISOs). Pertaining to privacy and confidentiality of data, each ISO is unwilling to disclose financial information, system topology, or control regulations to others. It is therefore not practical to gather all required information and perform operation decisions in a centralized pool. As an alternative approach to meet the challenges of centralized optimization methods, distributed optimization [14]-[26] have recently drawn more attention [16]. Reference [17] adopts enhanced Benders decomposition to solve the collaborative operation problem of networked microgrids with the local utility grid. This specific type of Benders cuts need to be formulated skillfully, and the decoupling manner is not intuitive to express the physical meaning of the system. Reference [18] employs a feasible region method to solve the dispatch problems of EPSs and DHSs independently. It is expected that the shape of the simplified and narrowed feasible region is as large as the exact feasible region, because it affects the conservativeness of the method distinctly. Based on the decentralized-agent communication mode, [19] introduces a $K-1$ algorithm to evaluate the reliability of systems with radial structure, but the effectiveness of the $K-1$ algorithm is not discussed in a loop structure [19]. Reference [20] applies the Lagrangian relaxation to optimal power flow scheduling of multi-area power systems. Moreover, a dynamic multiplier updating strategy is presented in [21]. Due to its convergence issues, the Lagrangian relaxation may impede practical applications in production.

The decentralized framework of the alternating direction method of multipliers (ADMM) can meet the task of contemporary wireless communications and networking [22]. This framework has been practically employed in optimization problems in recent years [23]-[26]. A power-heat-gas-coupling problem is solved by a novel distributed-consensus-ADMM in [23]. A dynamic average consensus algorithm is developed in this method for estimating the global information to overcome the drawback of conventional ADMM. Most of the papers mentioned above focus on the calculation performance of distributed algorithms. However, little attention is paid to the realistic process of communication and transmission. According to [16] and [27], most of the 42 disruption events affecting California ISOs were caused by failures of applications and communication from January 2012 to February 2012. This type of disruption event could lead to security risks and financial losses, and a poor customer experience could be bombarded with customer complaints. As a remedy, these operation risks can be potentially reduced by considering the instability or potential malfunctioning of the communication channels in a distributed algorithm. The classical distributed algorithms rely on limited available data offered by neighboring areas, and might not converge if the communication links are prone to failure. Communication delay is considered in [28], and the multi-area optimal power flow problem is solved by the asynchronous ADMM. Considering the different timescales of EPSs and DHSs, [29] proposes a distributed algorithm based on event-trigger to adapt the pattern of distributed calculation and asynchronous communication. A noisy ADMM is proposed in [30] with the presence of nodal errors during transmission, but the practical application effects are not yet discussed. An edge-based algorithm is provided in [31] for the network with unconnected union. The improvement is achieved at the cost of additional complexity and the convergence is guaranteed only in a milder and more practical connectivity condition.

Considering the need for a decentralized solution to the IEHS coordination and the possibility of communication packet loss, this paper proposes the relaxed ADMM (R-ADMM) for an IEHS over a lossy communication network. The contributions of this paper are summarized as follows.

1) This paper proposes a distributed coordination model for an IEHS to adapt to independent operation of different operators of the EPS and DHS. The R-ADMM is developed by applying the relaxed Peaceman-Rachford (P-R) splitting method to the Lagrangian dual of the original problem. While preserving the dispatch independence and guaranteeing the privacy of data, the proposed method can reach the same optimal solution as the centralized method. In contrast to the existing centralized algorithms, the distributed manner requires less computation resources, memory, and communication burden.

2) Considering the instability or potential malfunctioning of the communication channels, a binary probabilistic distribution model is used to describe communication failures caused by packet loss between neighboring areas. The R-ADMM still converges and shows faster convergence rates than the classical ones, embodying the calculation efficiency and robustness of the proposed method.

The rest of this paper is organized as follows. The coordination optimization model of an IEHS is introduced in Section II. In Section III, the coordination of an IEHS is formulated and solved in a decentralized manner using the distributed R-ADMM considering the impact of packet loss. In

Section IV, case studies are conducted to validate the robustness and effectiveness of the proposed distributed algorithm. Finally, conclusions are given in Section V.

II. Integrated Electrical and Heating System Coordination

The typical configuration of an IEHS is shown in Fig. 1. The IEHS is composed of an EPS and several DHSs with the characteristics of multiple agents. As different sub-systems are owned and controlled by different entities, it is not practical to solve problems in a centralized pool. The coordination model of an IEHS is presented in this section, and the distributed method is developed in the next section.

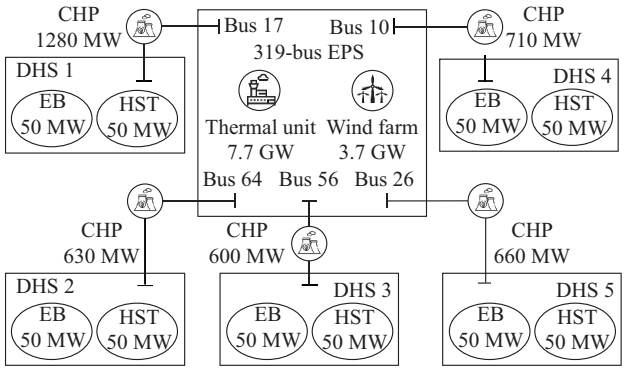

Fig. 1. Configuration of an IEHS.

A. Coordination Model of an IEHS

The coordination model of an IEHS minimizes the operation cost of the whole system, i.e., the sum of the EPS cost and DHS cost. The formulation of the coordination model of an IEHS can be expressed as:

$$\min_{\boldsymbol{x}^{\mathrm{EPS}}\in\Omega^{\mathrm{EPS}},\boldsymbol{y}_j^{\mathrm{DHS}}\in\Omega_j^{\mathrm{DHS}}} f(\boldsymbol{x}^{\mathrm{EPS}})+\sum_{j\in A^{\mathrm{DHS}}} g_j(\boldsymbol{y}_j^{\mathrm{DHS}}) \tag{1}$$

$$\text{s.t. } \boldsymbol{A}_j\boldsymbol{x}^{\mathrm{EPS}}+\boldsymbol{B}_j\boldsymbol{y}_j^{\mathrm{DHS}}=0 \quad j\in A^{\mathrm{DHS}} \tag{2}$$

Equation (2) is the coupling constraint of the EPS and DHS. It is assumed that gas turbine CHP units, whose power output is linearly proportional to the heat production, are installed in this paper. Then, (2) can be expressed as:

$$p_{h,t}^{\mathrm{CHP}}=\eta_h^{\mathrm{CHP}}q_{h,t}^{\mathrm{CHP}} \quad \forall h\in S_j^{\mathrm{CHP}}, j\in A^{\mathrm{DHS}}, t\in\mathcal{T} \tag{3}$$

Detailed models of the EPS and DHS are given in the following subsections.

B. Electric Power System Model

A typical EPS is composed of power generators, wind farms, and electric power loads. A DC power flow model is employed in the EPS, and the EPS model is subject to its physical and security constraints. The feasible region of an EPS is $\Omega^{\mathrm{EPS}}=\{p_{h,t}^{\mathrm{CHP}},p_{g,t}^{\mathrm{TU}},p_{w,t}^{\mathrm{wind}},ru_{g,t},rd_{g,t},\forall h\in S_j^{\mathrm{CHP}},g\in S^{\mathrm{TU}},w\in S^{\mathrm{wind}},n\in S^{\mathrm{bus}},t\in\mathcal{T},j\in A^{\mathrm{DHS}}\}$ subject to (4)-(13).

$$\sum_{j\in A^{\mathrm{DHS}}}\sum_{h\in S_j^{\mathrm{CHP}}} p_{h,t}^{\mathrm{CHP}}+\sum_{g\in S^{\mathrm{TU}}} p_{g,t}^{\mathrm{TU}}+\sum_{w\in S^{\mathrm{wind}}} p_{w,t}^{\mathrm{wind}}=\sum_{n\in S^{\mathrm{bus}}} D_{n,t} \tag{4}$$

$$\underline{F}_l\le\sum_{n\in S^{\mathrm{bus}}} SF_{l,n}\left(p_{h,t}^{\mathrm{CHP}}+\sum_{g\in S^{\mathrm{TU}}} p_{g,t}^{\mathrm{TU}}+\sum_{w\in S^{\mathrm{wind}}} p_{w,t}^{\mathrm{wind}}\right)\le\bar{F}_l \tag{5}$$

$$\underline{p}_h^{\mathrm{CHP}}\le p_{h,t}^{\mathrm{CHP}}\le\bar{p}_h^{\mathrm{CHP}} \tag{6}$$

$$\underline{p}_g^{\mathrm{TU}}\le p_{g,t}^{\mathrm{TU}}\le\bar{p}_g^{\mathrm{TU}} \tag{7}$$

$$0\le p_{w,t}^{\mathrm{wind}}\le\bar{p}_w^{\mathrm{wind}} \tag{8}$$

$$-RAMP_h^{\mathrm{down}}\cdot\Delta t\le p_{h,t}^{\mathrm{CHP}}-p_{h,t-1}^{\mathrm{CHP}}\le RAMP_h^{\mathrm{up}}\cdot\Delta t \tag{9}$$

$$-RAMP_g^{\mathrm{down}}\cdot\Delta t\le p_{g,t}^{\mathrm{TU}}-p_{g,t-1}^{\mathrm{TU}}\le RAMP_g^{\mathrm{up}}\cdot\Delta t \tag{10}$$

$$0\le rd_{g,t}\le RAMP_g^{\mathrm{down}}\cdot\Delta t \quad rd_{g,t}\le p_{g,t}^{\mathrm{TU}}-\underline{p}_g^{\mathrm{TU}} \tag{11}$$

$$0\le ru_{g,t}\le RAMP_g^{\mathrm{up}}\cdot\Delta t \quad ru_{g,t}\le\bar{p}_g^{\mathrm{TU}}-p_{g,t}^{\mathrm{TU}} \tag{12}$$

$$\begin{cases}\sum_{g\in S^{\mathrm{TU}}} ru_{g,t}\ge SR^{\mathrm{up}}\\ \sum_{g\in S^{\mathrm{TU}}} rd_{g,t}\ge SR^{\mathrm{down}}\end{cases} \tag{13}$$

where $\forall h\in S_j^{\mathrm{CHP}},g\in S^{\mathrm{TU}},w\in S^{\mathrm{wind}},n\in S^{\mathrm{bus}},l\in S^{\mathrm{line}},t\in\mathcal{T}$.

Equation (4) shows that the total power production and electric loads of the system remain balanced at all times. Inequation (5) represents network constraints that the transmission flows cannot exceed the transmission ability. Inequations (6), (7), and (8) represent the installed capacities of CHP units, thermal units, and wind power generators, respectively. Inequations (9) and (10) are the ramping rate constraints of CHP units and thermal units, respectively. Inequations (11) and (12) are upward/downward spinning reserve capacity constraints of thermal units. Inequation (13) describes the system-wide upward and downward spinning reserve capacity requirements.

The coupling connection of CHP is decomposed to the electric power output of CHPs for the EPS and the heat output of CHPs for the DHSs [32]. Note that the weight of coupling coefficient of electric power output and heat output of CHPs is typically small, which can be neglected. The electric generation cost of thermal units and CHP units and the penalty term for wind power spillage can be described by a convex quadratic function. Hence, the total cost of an EPS to be minimized is the sum of these three parts as:

$$\begin{aligned}f(\boldsymbol{x}^{\mathrm{EPS}})=\sum_{t\in\mathcal{T}}\Bigg[&\sum_{g\in S^{\mathrm{TU}}} b_{0,g}+b_{1,g}p_{g,t}^{\mathrm{TU}}+b_{2,g}(p_{g,t}^{\mathrm{TU}})^2+\\&\sum_{h\in S_j^{\mathrm{CHP}}} a_{0,h}+a_{1,h}p_{h,t}^{\mathrm{CHP}}+a_{2,h}(p_{h,t}^{\mathrm{CHP}})^2+\\&\sum_{w\in S^{\mathrm{wind}}}\delta_w(\bar{p}_{w,t}^{\mathrm{wind}}-p_{w,t}^{\mathrm{wind}})^2\Bigg]\end{aligned} \tag{14}$$

C. District Heating System Model

The DHS model consists of heat sources, supply/return heating pipeline networks, and heat loads. Heat is produced by CHP units, EBs and HSTs. Water is heated and transported to heat consumers through pipeline networks. The hydraulic regimes of a DHS are described by the mass flows inside pipelines. The thermal part of a DHS considers the thermal energy and temperature. A node method [33] is used to simulate the temperature dynamics in a DHS, including time delays and heat losses. For each DHS j, $j\in A^{\mathrm{DHS}}$, the feasible region is $\Omega_j^{\mathrm{DHS}}=\{q_{e,t}^{\mathrm{EB}},p_{e,t}^{\mathrm{EB}},\boldsymbol{\varphi}_{s,t}^{\mathrm{HST}},q_{s,t}^{\mathrm{HST}},q_{h,t}^{\mathrm{CHP}},\tau_{i,t}^{\mathrm{NS}},\tau_{i,t}^{\mathrm{NR}},\tau_{b,t}^{\mathrm{PS,in}},\tau_{b,t}^{\mathrm{PS,out}},$

$\tau_{b,t}^{\mathrm{PR,in}}, \tau_{b,t}^{\mathrm{PR,out}}, \tau_{b,t}^{\mathrm{'PS,out}}, \tau_{b,t}^{\mathrm{'PR,out}}, \forall e \in I^{\mathrm{EB}}, s \in I^{\mathrm{HST}}, h \in S^{\mathrm{CHP}}, i \in I^{\mathrm{node}}, b \in I^{\mathrm{pipe}}, t \in \mathcal{T}\}$ subject to (15)-(29).

$$q_{e,t}^{\mathrm{EB}} = \eta_e^{\mathrm{EB}} p_{e,t}^{\mathrm{EB}} \tag{15}$$

$$0 \le p_{e,t}^{\mathrm{EB}} \le \bar{p}_e^{\mathrm{EB}} \tag{16}$$

$$\boldsymbol{C}\boldsymbol{\varphi}_{s,t}^{\mathrm{HST}} \le \boldsymbol{d} \tag{17}$$

$$\sum_{h \in S_j^{\mathrm{CHP}}} q_{h,t}^{\mathrm{CHP}} + \sum_{e \in I^{\mathrm{EB}}} p_{e,t}^{\mathrm{EB}} + \sum_{s \in I^{\mathrm{HST}}} q_{s,t}^{\mathrm{HST}} = cm_{\mu,t}^{\mathrm{HS}} (\tau_{n,t}^{\mathrm{NS}} - \tau_{n,t}^{\mathrm{NR}}) \tag{18}$$

$$\underline{\tau}_{n,t}^{\mathrm{NS}} \le \tau_{n,t}^{\mathrm{NS}} \le \bar{\tau}_{n,t}^{\mathrm{NS}} \tag{19}$$

$$cm_{v,t}^{\mathrm{HES}} (\tau_{m,t}^{\mathrm{NS}} - \tau_{m,t}^{\mathrm{NR}}) = H_{v,t}^{\mathrm{HES}} \tag{20}$$

$$\underline{\tau}_{m,t}^{\mathrm{NR}} \le \tau_{m,t}^{\mathrm{NR}} \le \bar{\tau}_{m,t}^{\mathrm{NR}} \tag{21}$$

$$\sum_{b^- \in S_i^{\mathrm{pipe-}}} (\tau_{b^-,t}^{\mathrm{PS,out}} m_{b^-,t}^{\mathrm{PS}}) = \tau_{i,t}^{\mathrm{NS}} \sum_{b^- \in S_i^{\mathrm{pipe-}}} m_{b^-,t}^{\mathrm{PS}} \tag{22}$$

$$\sum_{b^+ \in S_i^{\mathrm{pipe+}}} (\tau_{b^+,t}^{\mathrm{PR,out}} m_{b^+,t}^{\mathrm{PR}}) = \tau_{i,t}^{\mathrm{NR}} \sum_{b^+ \in S_i^{\mathrm{pipe+}}} m_{b^+,t}^{\mathrm{PR}} \tag{23}$$

$$\tau_{b^+,t}^{\mathrm{PS,in}} = \tau_{i,t}^{\mathrm{NS}} \tag{24}$$

$$\tau_{b^-,t}^{\mathrm{PR,in}} = \tau_{i,t}^{\mathrm{NR}} \tag{25}$$

$$\tau_{b,t}^{\mathrm{'PS,out}} = \sum_{k=t-\phi_{b,t}}^{t-\gamma_{b,t}} K_{b,t,k} \tau_{b,k}^{\mathrm{PS,in}} \tag{26}$$

$$\tau_{b,t}^{\mathrm{'PR,out}} = \sum_{k=t-\phi_{b,t}}^{t-\gamma_{b,t}} K_{b,t,k} \tau_{b,k}^{\mathrm{PR,in}} \tag{27}$$

$$\tau_{b,t}^{\mathrm{PS,out}} = \tau_t^{\mathrm{amb}} + (\tau_{b,t}^{\mathrm{'PS,out}} - \tau_t^{\mathrm{amb}}) \cdot \exp\left[-\frac{\lambda_b \Delta t}{A_b \rho^{\mathrm{ms}} c} \left(\gamma_{b,t} + \frac{1}{2} + \frac{S_{b,t} - R_{b,t}}{m_{b,t-\gamma_{b,t}}^{\mathrm{PS}} \Delta t} \right) \right] \tag{28}$$

$$\tau_{b,t}^{\mathrm{PR,out}} = \tau_t^{\mathrm{amb}} + (\tau_{b,t}^{\mathrm{'PR,out}} - \tau_t^{\mathrm{amb}}) \cdot \exp\left(-\frac{\lambda_b \Delta t}{A_b \rho^{\mathrm{ms}} c} \left(\gamma_{b,t} + \frac{1}{2} + \frac{S_{b,t} - R_{b,t}}{m_{b,t-\gamma_{b,t}}^{\mathrm{PS}} \Delta t} \right) \right)$$
$$\forall e \in I^{\mathrm{EB}}, s \in I^{\mathrm{HST}}, h \in S_j^{\mathrm{CHP}}, n \in Nd_\mu^{\mathrm{HS}}, \mu \in I^{\mathrm{HS}}, m \in Nd_v^{\mathrm{HES}}, i \in I^{\mathrm{node}}, b^- \in S_i^{\mathrm{pipe-}}, b^+ \in S_i^{\mathrm{pipe+}}, v \in I^{\mathrm{HES}}, b \in I^{\mathrm{pipe}}, t \in \mathcal{T} \tag{29}$$

Equations and inequations (15)-(19) represent the model of heat sources. The heat output of an EB is linearly related to electricity consumption in (15), and the limit of its electricity consumption is denoted in (16). Inequation (17) represents an abstract model of an HST, described as a three-layer mixing temperature model according to [6]. Then, the heat output of heat sources in a heat station is used to heat the flow in (18). Inequation (19) represents that the temperatures of the heat station in the supply network are limited to avoid steam formation.

Equation (20) and inequation (21) represent the model of heat loads. The heat exchanger stations are modeled as heat loads in (20), and the temperatures of the heat exchanger stations in the return network are bounded in (21).

Equations (22)-(25) are DHS constraints. Equations (22) and (23) describe temperature mixing in the supply and return network due to the law of energy conservation. Additionally, the temperature of the mass flow from a node is equal to that of the water flowing into the pipe, as described in (24) and (25).

Equations (26)-(29) represent temperature dynamics and heat loss constraints. Temperatures change due to time delays in transmission. In (26) and (27), the outlet temperatures can be denoted by the average temperatures outflowing from the pipeline during Δt without heat loss. Besides, the temperature drops pertaining to heat losses are caused by ambient temperatures, as shown in (28) and (29). More details can be found in [9].

The operation cost of DHS j, $j \in \mathrm{A}^{\mathrm{DHS}}$, is the heat generation cost of CHPs, which can be expressed as a quadratic function as:

$$g_j(\boldsymbol{y}_j^{\mathrm{DHS}}) = \sum_{t \in \mathcal{T}} a_{3,h} q_{h,t}^{\mathrm{CHP}} + a_{4,h} (q_{h,t}^{\mathrm{CHP}})^2 \quad \forall h \in S_j^{\mathrm{CHP}} \tag{30}$$

III. Distributed R-ADMM Considering Packet Loss

The coordination model of an IEHS is denoted in (1) and (2). For the EPS, the objective function is (14) with constraints (4)-(13). For the DHS, the objective function is (30) with constraints (15)-(29). Note that the coupling constraint in (2) makes it difficult to solve EPS subproblems and DHS subproblems independently. Therefore, a distributed solution is introduced in this section.

A. Distributed R-ADMM

The classic ADMM is closely related to the relaxed P-R splitting method [16], [22], which has a faster convergence rate than the classic ADMM [34]. The calculation procedure for the distributed R-ADMM is formulated as follows by employing relaxed P-R splitting.

By relaxing (2), the Lagrangian function of the primal problem is constructed as:

$$L_\rho(\boldsymbol{x}^{\mathrm{EPS}}, \boldsymbol{y}^{\mathrm{DHS}}, \boldsymbol{\lambda}_j) = f(\boldsymbol{x}^{\mathrm{EPS}}) + \sum_{j \in A^{\mathrm{DHS}}} g_j(\boldsymbol{y}_j^{\mathrm{DHS}}) + \sum_{j \in A^{\mathrm{DHS}}} \left[-\boldsymbol{\lambda}_j^{\mathrm{T}} (\boldsymbol{A}_j \boldsymbol{x}^{\mathrm{EPS}} - \boldsymbol{B}_j \boldsymbol{y}_j^{\mathrm{DHS}}) + \frac{\rho}{2} \left\| \boldsymbol{A}_j \boldsymbol{x}^{\mathrm{EPS}} - \boldsymbol{B}_j \boldsymbol{y}_j^{\mathrm{DHS}} \right\|_2^2 \right] \tag{31}$$

First, given the iterative form of the classic ADMM, for $j \in A^{\mathrm{DHS}}$, the EPS and DHS subproblems are formulated as:

$$\boldsymbol{x}^{\mathrm{EPS}}(k+1) = \arg\min_{\boldsymbol{x}^{\mathrm{EPS}} \in \Omega^{\mathrm{EPS}}} L_\rho(\boldsymbol{x}^{\mathrm{EPS}}, \boldsymbol{y}_j^{\mathrm{DHS}}(k), \boldsymbol{\lambda}_j(k)) \tag{32}$$

$$\boldsymbol{y}_j^{\mathrm{DHS}}(k+1) = \arg\min_{\boldsymbol{y}_j^{\mathrm{DHS}} \in \Omega_j^{\mathrm{DHS}}} L_\rho(\boldsymbol{x}^{\mathrm{EPS}}(k+1), \boldsymbol{y}_j^{\mathrm{DHS}}, \boldsymbol{\lambda}_j(k)) \tag{33}$$

Second, by leveraging the relaxed P-R splitting method to the Lagrangian dual problem of (1) and (2), the R-ADMM is developed. Then, the EPS and DHS subproblems can be reformulated as:

$$\min_{\boldsymbol{x}^{\mathrm{EPS}} \in \Omega^{\mathrm{EPS}}} \left\{ f(\boldsymbol{x}^{\mathrm{EPS}}) - \sum_{j \in A^{\mathrm{DHS}}} \left((\boldsymbol{z}_j^{\mathrm{EPS}}(k))^{\mathrm{T}} \boldsymbol{A}_j \boldsymbol{x}^{\mathrm{EPS}} + \frac{\rho}{2} \left\| \boldsymbol{A}_j \boldsymbol{x}^{\mathrm{EPS}} \right\|_2^2 \right) \right\} \tag{34}$$

$$\min_{\boldsymbol{y}_j^{\mathrm{DHS}} \in \Omega_j^{\mathrm{DHS}}} \left\{ g_j(\boldsymbol{y}_j^{\mathrm{DHS}}) - (\boldsymbol{z}_j^{\mathrm{DHS}}(k))^{\mathrm{T}} \boldsymbol{B}_j \boldsymbol{y}_j^{\mathrm{DHS}} + \frac{\rho}{2} \left\| \boldsymbol{B}_j \boldsymbol{y}_j^{\mathrm{DHS}} \right\|_2^2 \right\} \tag{35}$$

where $j \in A^{\mathrm{DHS}}$; and $\boldsymbol{z}_j^{\mathrm{EPS}}$ and $\boldsymbol{z}_j^{\mathrm{DHS}}$ are the auxiliary multipliers

in this paper and have the same dimension as the Lagrangian multipliers $\boldsymbol{\lambda}_j$ in the Lagrangian function (31).

The relaxed P-R splitting method converts the original optimization into finding a fixed point of an operator. In fact, the vector $\boldsymbol{z}$ is the fixed point of the relaxed P-R splitting operator T_{PRS}, which can be iteratively calculated by $\boldsymbol{z}(k+1)=(1-\alpha)\boldsymbol{z}(k)+\alpha T_{\text{PRS}}\boldsymbol{z}(k)$ [35]. $\boldsymbol{z}$ consists of $\boldsymbol{z}_j^{\text{EPS}}$ and $\boldsymbol{z}_j^{\text{DHS}}$. By applying P-R splitting, the auxiliary multipliers in (34) and (35) can be calculated as (36) and (37), where $\alpha\in[0,1]$.

$$\boldsymbol{z}_j^{\text{EPS}}(k+1)=(1-\alpha)\boldsymbol{z}_j^{\text{EPS}}(k)-\alpha\boldsymbol{z}_j^{\text{DHS}}(k)+2\alpha\rho\boldsymbol{B}_j\boldsymbol{y}_j^{\text{DHS}}(k) \quad (36)$$

$$\boldsymbol{z}_j^{\text{DHS}}(k+1)=(1-\alpha)\boldsymbol{z}_j^{\text{DHS}}(k)-\alpha\boldsymbol{z}_j^{\text{EPS}}(k)+2\alpha\rho\boldsymbol{A}_j\boldsymbol{x}^{\text{EPS}}(k) \quad (37)$$

It is practically reasonable to assume the communication link between an EPS and a DHS is connected. Note that for an EPS, $\boldsymbol{z}_j^{\text{DHS}}$ and $\boldsymbol{B}_j\boldsymbol{y}_j^{\text{DHS}}$ are updated by the adjacent DHS j, while for a DHS, $\boldsymbol{z}_j^{\text{EPS}}$ and $\boldsymbol{A}_j\boldsymbol{x}^{\text{EPS}}$ are updated by the EPS. Accordingly, (36) and (37) can be reformulated as:

$$\boldsymbol{z}_j^{\text{EPS}}(k+1)=(1-\alpha)\boldsymbol{z}_j^{\text{EPS}}(k)+\alpha\boldsymbol{U}_j^{\text{h}\to\text{e}}(k) \quad (38)$$

$$\boldsymbol{U}_j^{\text{h}\to\text{e}}(k)=-\boldsymbol{z}_j^{\text{DHS}}(k)+2\rho\boldsymbol{B}_j\boldsymbol{y}_j^{\text{DHS}}(k) \quad (39)$$

$$\boldsymbol{z}_j^{\text{DHS}}(k+1)=(1-\alpha)\boldsymbol{z}_j^{\text{DHS}}(k)+\alpha\boldsymbol{U}_j^{\text{e}\to\text{h}}(k) \quad (40)$$

$$\boldsymbol{U}_j^{\text{e}\to\text{h}}(k)=-\boldsymbol{z}_j^{\text{EPS}}(k)+2\rho\boldsymbol{A}_j\boldsymbol{x}^{\text{EPS}}(k) \quad (41)$$

Like most distributed algorithms, the proposed R-ADMM can solve subproblems separately with limited boundary information exchange between an EPS and its adjacent DHSs.

The procedure for solving each subproblem of the R-ADMM is summarized as follows.

Step 1: For an EPS, solve the subproblem denoted by (34). Then, update boundary information $\boldsymbol{U}_j^{\text{e}\to\text{h}}$ by (41), and transmit it to DHS j. After receiving boundary information from a DHS, the EPS updates auxiliary multipliers by (38).

Step 2: For each DHS, solve the subproblem denoted by (35). Then, update boundary information $\boldsymbol{U}_j^{\text{h}\to\text{e}}$ by (39), and transmit it to the EPS. After receiving boundary information from the EPS, the DHS updates auxiliary multipliers by (40).

The R-ADMM maintains a splitting framework of the P-R splitting method. Only requiring minor data to be exchanged, the proposed method decomposes IEHS coordination problems into smaller separable subproblems (34) and (35). It is noteworthy that the distributed R-ADMM degenerates to the classic ADMM for $\alpha=0.5$. If the objective functions f and g_j are closed and convex, the Lagrangian dual problem of (1) and (2) has no duality gap. For $\alpha\in[0,1]$ and $\rho>0$, the R-ADMM converges to the optimal solution for any $\boldsymbol{z}_j^{\text{EPS}}(\boldsymbol{0})$ and $\boldsymbol{z}_j^{\text{DHS}}(\boldsymbol{0})$ [35].

B. Communication Packet Loss

The algorithm illustrated previously works under the assumption of original reliable communication channels. In a lossy communication network, the boundary information may not be received from its neighboring areas. It means the event of packet loss occurs randomly with a probability. The auxiliary multipliers can be updated only if the operators receive the boundary information. The communication failures caused by packet loss can be described using a binary probabilistic distribution as:

$$\begin{cases}\mathbb{P}\left[L_j^{\text{e}\to\text{h}}=1\right]=p_j^{\text{e}\to\text{h}}\\ \mathbb{P}\left[L_j^{\text{e}\to\text{h}}=0\right]=1-p_j^{\text{e}\to\text{h}}\end{cases} \quad (42)$$

If the communication between the EPS and the j^{th} DHS fails with probability $p_j^{\text{e}\to\text{h}}$, let $L_j^{\text{e}\to\text{h}}=1$, and keep the auxiliary multiplier $\boldsymbol{z}$ unchanged. Otherwise, let $L_j^{\text{e}\to\text{h}}=0$, and update $\boldsymbol{z}$ by (38) and (40). Then, (38) and (40) are modified as:

$$\boldsymbol{z}_j^{\text{EPS}}(k+1)=L_j^{\text{h}\to\text{e}}(k)\boldsymbol{z}_j^{\text{EPS}}(k)+\left[1-L_j^{\text{h}\to\text{e}}(k)\right]\left[(1-\alpha)\boldsymbol{z}_j^{\text{EPS}}(k)+\alpha\boldsymbol{U}_j^{\text{h}\to\text{e}}(k)\right] \quad (43)$$

$$\boldsymbol{z}_j^{\text{DHS}}(k+1)=L_j^{\text{e}\to\text{h}}(k)\boldsymbol{z}_j^{\text{DHS}}(k)+\left[1-L_j^{\text{e}\to\text{h}}(k)\right]\left[(1-\alpha)\boldsymbol{z}_j^{\text{DHS}}(k)+\alpha\boldsymbol{U}_j^{\text{e}\to\text{h}}(k)\right] \quad (44)$$

The value of relaxed step size α is tunable in the R-ADMM, and the influence of the setting of α is shown in Section IV. Considering packet losses, for $\alpha\in[0,1]$ and $\rho>0$, the distributed R-ADMM converges almost surely to the optimal solution of (1) and (2) for any $\boldsymbol{z}_j^{\text{EPS}}(\boldsymbol{0})$ and $\boldsymbol{z}_j^{\text{DHS}}(\boldsymbol{0})$ [35].

The termination criterion is set as follows in terms of the primal residual $\boldsymbol{r}$ and the dual residual $\boldsymbol{s}$:

$$\begin{cases}\left\|\boldsymbol{r}(k)\right\|=\sum\limits_{j\in\text{A}^{\text{DHS}}}\left\|\boldsymbol{A}_j\boldsymbol{x}^{\text{EPS}}-\boldsymbol{B}_j\boldsymbol{y}_j^{\text{DHS}}\right\|\le\varepsilon^{\text{pri}}\\ \left\|\boldsymbol{s}(k)\right\|=\left\|\rho\boldsymbol{A}_j^{\text{T}}\boldsymbol{B}_j(\boldsymbol{y}_j^{\text{DHS}}(k)-\boldsymbol{y}_j^{\text{DHS}}(k-1))\right\|\le\varepsilon^{\text{dual}}\end{cases} \quad (45)$$

A flowchart of the distributed R-ADMM considering packet loss is summarized in Fig. 2.

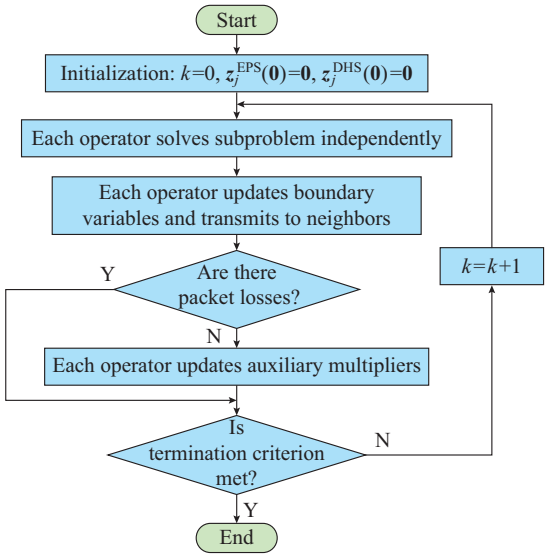

Fig. 2. Flowchart of distributed R-ADMM considering communication packet loss.

IV. Case Studies

Numerical experiments of two IEHSs are conducted to verify the effectiveness and robustness of the proposed distributed R-ADMM. The configurations of the test systems are shown in Table I.

Case I is a test system consisting of an IEEE 6-bus EPS and 6-node DHS. This case is tested to illustrate the computation accuracy of the proposed R-ADMM. In addition, the robustness of the algorithm is tested for different values of relaxed step size α and packet loss probability p. The other

case is composed of an EPS and several DHSs, whose prototypes are practical systems in the northeastern China. This case is presented to compare the distributed R-ADMM and the classic ADMM in terms of performance in convergence and calculation.

All tests are performed on a computer with four processors running at 3.4 GHz and 8 GB of RAM. The quadratic program is solved by CPLEX running on MATLAB R2018a. The initial values of the parameters of the R-ADMM are set to $\boldsymbol{z}_j^{\mathrm{EPS}}(\mathbf{0})=\mathbf{0}$, $\boldsymbol{z}_j^{\mathrm{DHS}}(\mathbf{0})=\mathbf{0}$, and $\rho=0.02$. The termination criteria $\varepsilon^{\mathrm{pri}}$ and $\varepsilon^{\mathrm{dual}}$ are set to 10^{-3} and 10^{-5}, respectively.

TABLE I
CONFIGURATIONS OF TEST SYSTEMS

Case	EPS				Coupling units	DHS				
	Bus No.	Line No.	Thermal unit No.	Wind farm No.	CHP No.	EB No.	HST No.	Node No.	Pipeline No.	HES No.
I	6	7	2	1	1	1	1	6	5	3
II	319	431	60	34	5	1	1	8	7	4

A. Case I: IEHS with a 6-bus EPS and a 6-node DHS

In Case I, the small-scale IEHS comprises a 6-bus EPS and a 6-node DHS connected by a CHP unit. The EPS contains two thermal units, a wind farm, and a CHP unit connected to Bus 6. In the DHS, heat sources including a CHP unit, an EB and an HST are connected to Node 1 to fulfill heat loads at Buses 4, 5, and 6. The configuration of the system in Case I is provided in Table I and Fig. 3, where the red and blue lines are the supply and return pipes, respectively. More details can be found in [36].

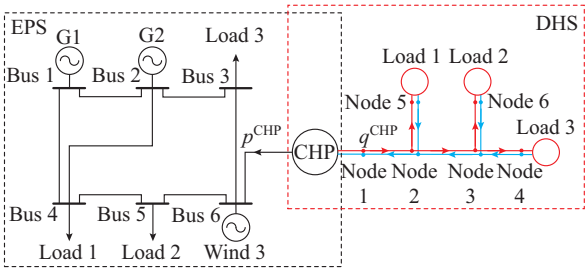

Fig. 3. Configuration of IEHS in Case I.

In the R-ADMM, $\alpha=1$, and $p_j^{\mathrm{e}\to\mathrm{h}}=p_j^{\mathrm{h}\to\mathrm{e}}=p=0.05$. The system is tested for hourly coordination over 24 hours. The primal residuals and dual residuals converge to 7.195×10^{-6} and 2.463×10^{-6} in 25 iterations, respectively, consuming 1.084 s. The hourly dispatches of electric power and heating power in Case I are plotted in Fig. 4.

In Fig. 4 (a), the heat loads and available wind power are on-peak at nighttime, while the electricity loads are on-peak at daytime. More electric power of thermal units and CHP units is generated from 8 a.m. to 8 p.m. in order to satisfy the electricity demand at daytime. By exploiting the heat storage capacities of pipelines and an HST, the heat output of CHP units is reduced at nighttime to accommodate wind integration. Therefore, the sum of heat output is not always equal to the heat loads in each period, as shown in Fig. 4(b).

Different values of α are set to analyze the impact on convergence rates of the distributed R-ADMM with fixed packet loss probability $p_j^{\mathrm{e}\to\mathrm{h}}=p_j^{\mathrm{h}\to\mathrm{e}}=p=0.05$. Figure 5 depicts the evolution of relative errors for different values of α in Case I. The relative errors are computed as the ratio between the absolute errors and the optimal solution of the centralized method. Considering the randomness of the communication packet loss, the tests are performed over 100 Monte Carlo simulations. As shown in Fig. 5, the relative errors fluctuate slightly. This fluctuation is caused by information exchange to mitigate the mismatch with x^*, behaving similarly to the Lagrangian methods. The R-ADMM degenerates into the general ADMM if $\alpha=0.5$ and converges more quickly than the classic ADMM. In addition, the convergence rates are improved with larger α. In other words, by choosing the relaxed step size properly, the convergence performance can be improved.

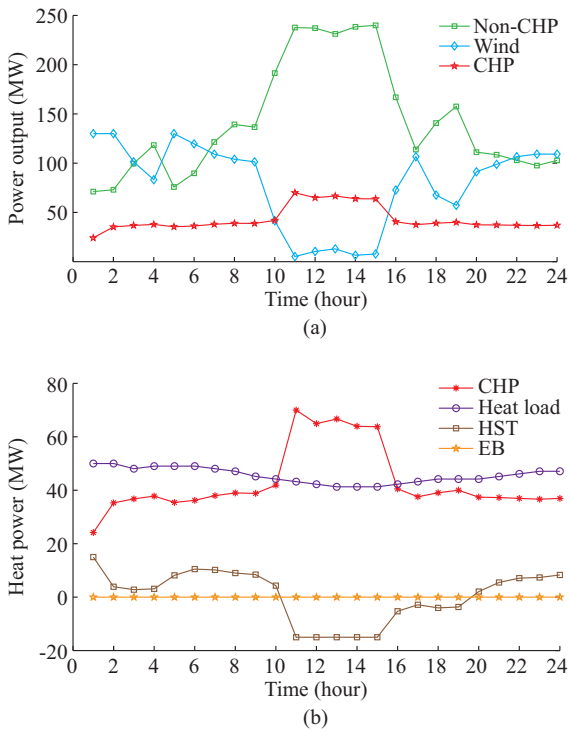

Fig. 4. Hourly dispatches of electric power and heating power in Case I. (a) Electric output. (b) Heat output.

The communication packet losses occur randomly in the following case. For different values of packet loss probability $p_j^{\mathrm{e}\to\mathrm{h}}=p_j^{\mathrm{h}\to\mathrm{e}}=p$ with fixed $\alpha=1$, the evolution of relative errors is reported in Fig. 6.

Similarly, 100 Monte Carlo tests are performed. In these

scenarios with stochastic communication failure, the boundary information cannot be updated in time. The packet losses among neighbors affect the computation negatively. The relative error drops the most quickly without any packet loss, as shown in Fig. 6. The convergence performance is deteriorated by the increase of communication failure probability.

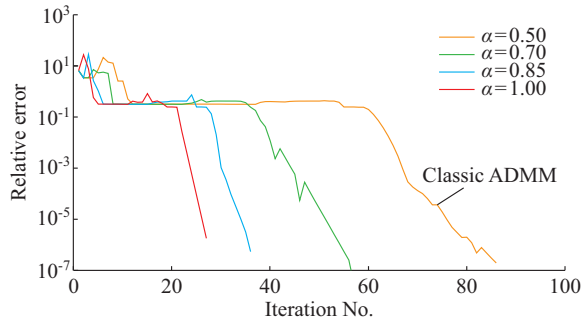

Fig. 5. Effect on evolution of relative errors for different values of α in Case I.

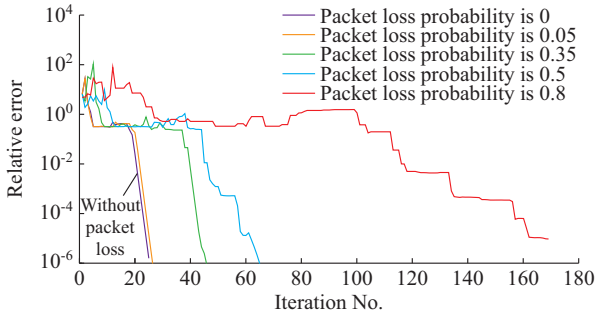

Fig. 6. Effect on evolution of relative errors for different values of p in Case I.

B. Case II: IEHS with a 319-bus EPS and 5 8-node DHSs

A large-scale IEHS with a 319-bus EPS and 5 8-node DHSs is investigated. The EPS is equipped with 60 thermal units, 34 wind farms, and 5 CHP units with a total generation capacity of 7.7 GW, 3.7 GW, and 3880 MW, respectively. This EPS is connected to five DHSs through CHP units. Each DHS consists of one heat source, seven pipes, and four heat loads. The system configuration is depicted in Fig. 1. More details can be found in [37] and [38].

With fixed $\alpha=0.5$ and $\alpha=1$, the results of the classic ADMM and the R-ADMM with different packet loss probabilities $p_j^{e\to h}=p_j^{h\to e}=p$ are compared in Table II. The centralized method is used as the benchmark for the distributed algorithm. The calculation performance is characterized by the number of iterations and CPU time. The computation accuracy is described by relative errors, defined as the absolute errors divided by the optimal solution x^*. The financial expenditure is indicated by the total cost.

With a low probability of communication failures, i.e., $p=0.05$, both the ADMM and R-ADMM can reach nearly the same solution as the centralized method with favorable convergence performance. In this scenario, the R-ADMM needs 55 iterations to reach the optimal solution, which is less than the ADMM. Compared to the ADMM, the R-ADMM saves 129.9 s of computation time. In this communication scenario with losses, the "out-of-date" boundary messages used in the latest updating affect the computation accuracy. The relative errors of the ADMM are larger than those of the R-ADMM, which verifies that communication failures have a larger negative impact on the ADMM. Therefore, the R-ADMM shows better performance in calculation and convergence than the ADMM.

For a larger packet loss probability, e.g., $p=0.5$, the R-ADMM converges in 102 iterations, consuming 247.4 s. With $p=0.8$, the primal residuals and dual residuals present oscillations that make the ADMM not converge. In contrast, the R-ADMM could still achieve nearly the same optimal solution, which validates the robustness of the R-ADMM under negative effects of packet loss. As shown in Table II, more frequent communication failures would lead to the increase of both the calculation time and the number of iterations.

TABLE II
COMPARISON OF RESULTS OF DIFFERENT METHODS IN DIFFERENT PACKET LOSS SCENARIOS

Method	Probability	No. of iterations	CPU time (s)	Relative error	Total cost ($)
Centralized method	$p=0$	-	1.594×10^{1}	-	66645.6886
ADMM ($\alpha=0.5$)	$p=0.05$	109	262.5	2.163×10^{-5}	66645.6806
	$p=0.50$	209	499.7	1.969×10^{-5}	66645.6839
	$p=0.80$	No convergence	-	-	-
R-ADMM ($\alpha=1$)	$p=0.05$	55	132.6	1.446×10^{-5}	66645.6851
	$p=0.50$	102	247.4	1.390×10^{-5}	66645.6962
	$p=0.80$	298	711.2	1.759×10^{-5}	66645.6911

In the next test, the probabilities of communication failures for different pairs of sub-systems are set as different values, as shown in Table III.

In this communication scenario, the R-ADMM meets the termination criterion in 165 iterations consuming 401.3 s. The relative errors and total financial expenditures are 4.614×10^{-5} and \$66645.7014, respectively. Conversely, the classic ADMM does not converge. The effectiveness and robustness of the R-ADMM are further clarified by the evolution of the dual residuals and primal residuals, reflecting the optimality and feasibility, respectively. The evolution of residuals by the R-ADMM and the ADMM is depicted in Fig. 7 and Fig. 8, respectively.

As shown in Fig. 7, the primal residuals and dual residuals of the R-ADMM fall below 10^{-3} and 10^{-5}, respectively, after 165 iterations. The R-ADMM is robust to random pack-

et loss. In Fig. 8, the evolution of residuals by the ADMM exhibits unstable oscillation. The classic ADMM may fail to converge in the scenarios with high probability of packet loss.

TABLE III
VALUES OF DIFFERENT PACKET LOSS PROBABILITIES

DHS	Packet loss probability
DHS 1	$p_1^{h\to e}=0.8$, $p_1^{e\to h}=0.9$
DHS 2	$p_2^{h\to e}=0.8$, $p_2^{e\to h}=0.9$
DHS 3	$p_3^{h\to e}=0.35$, $p_3^{e\to h}=0.9$
DHS 4	$p_4^{h\to e}=0.35$, $p_4^{e\to h}=0.65$
DHS 5	$p_5^{h\to e}=0.35$, $p_5^{e\to h}=0.65$

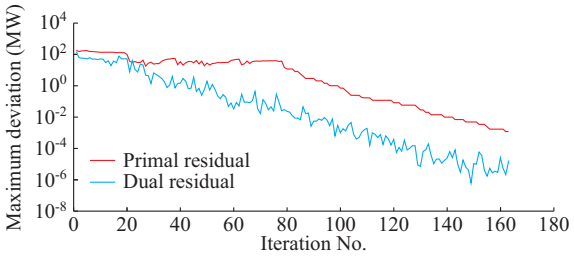

Fig. 7. Evolution of primal residuals and dual residuals of R-ADMM ($\alpha=1$) in Case II.

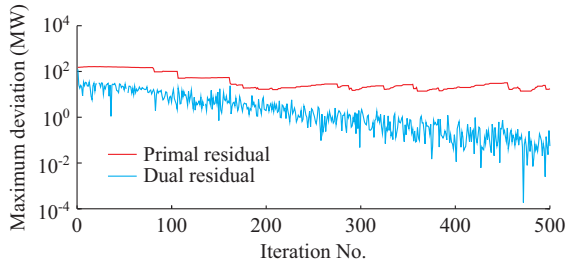

Fig. 8. Evolution of primal residuals and dual residuals of the ADMM ($\alpha=0.5$) in Case II.

V. CONCLUSION

This paper proposes a distributed R-ADMM algorithm for hedging communication packet loss in the economic dispatch of IEHS. The quasi-dynamic temperature changes are considered to account for the heat storage of pipelines in a DHS to integrate more wind power generation. The IEHS dispatch procedure is performed in a decentralized manner without any centrally coordinated operators. The R-ADMM is derived by applying the relaxed P-R splitting method to the Lagrangian dual problem. Two test systems with probabilistic communication loss are simulated to validate the effectiveness and robustness of the proposed algorithm, and the following conclusions are drawn:

1) The distributed R-ADMM still converges to the optimal solution of the centralized method even with communication failures. The effectiveness of the proposed R-ADMM is validated in the test results.

2) The convergence rate becomes slower with increasing probability p. Besides, suitably choosing α can lead to a better convergence rate for a fixed p.

3) The R-ADMM perform outperforms the classic ADMM in terms of computation time and convergence performance. In cases with high probability of packet loss, the R-ADMM can still converge while the classic ADMM probably can not.

Future works will incorporate additional communication and transmission conditions such as nodal errors, time delays, and false data injection attacks, which are of great significance for realizing efficient and robust communication and transmission for multi-agent systems.

REFERENCES

[1] Z. Pan, Q. Guo, and H. Sun, "Feasible region method based integrated heat and electricity dispatch considering building thermal inertia," *Applied Energy*, vol. 192, no. 15, pp. 395-407, Apr. 2017.
[2] J. Li, F. Cai, L. Qiao *et al.*, *2014 China Wind Power Review and Outlook*. Beijing: Chinese Renewable Energy Industries Association (CREIA), 2014.
[3] G. Papaefthymiou, B. Hasche, and C. Nabe, "Potential of heat pumps for demand side management and wind power integration in the German electricity market," *IEEE Transactions on Sustainable Energy*, vol. 3, no. 4, pp. 636-642, Oct. 2012.
[4] L. Yang, X. Zhang, and P. Gao, "Research on heat and electricity coordinated dispatch model for better integration of wind power based on electric boiler with thermal storage," *IET Generation, Transmission and Distribution*, vol. 12, pp. 3736-3743, Aug. 2018.
[5] N. Zhang, X. Lu, M. B. McElroy *et al.*, "Reducing curtailment of wind electricity in China by employing electric boilers for heat and pumped hydro for energy storage," *Applied Energy*, vol. 184, no. 15. pp. 987-994, Dec. 2016.
[6] X. Chen, C. Kang, M. O'Malley *et al.*, "Increasing the flexibility of combined heat and power for wind power integration in China: modeling and implications," *IEEE Transactions on Power Systems*, vol. 30, no. 4, pp. 1848-1857, Jul. 2015.
[7] X. Gou, Q. Chen, K. Hu *et al.*, "Optimal planning of capacities and distribution of electric heater and heat storage for reduction of wind power curtailment in power systems," *Energy*, vol. 160, no. 1, pp. 763-773, Oct. 2018.
[8] Z. Li, W. Wu, M. Shahidehpour *et al.*, "Combined heat and power dispatch considering pipeline energy storage of district heating network," *IEEE Transactions on Sustainable Energy*, vol. 7, no. 1, pp. 12-22, Jan. 2016.
[9] W. Gu, J. Wang, S. Lu *et al.*, "Optimal operation for integrated energy system considering thermal inertia of district heating network and buildings," *Applied Energy*, vol. 199, no.1, pp. 234-246, Aug. 2017.
[10] A. Haghrah, M. Nazari-Heris, and B. Mohammadi-Ivatloo, "Solving combined heat and power economic dispatch problem using real coded genetic algorithm with improved Mühlenbein mutation," *Applied Thermal Engineering*, vol. 99, no. 25, pp. 465-475, Apr. 2016.
[11] T. Nguyen and D. Vo, "Improved particle swarm optimization for combined heat and power economic dispatch," *Scientia Iranica*, vol. 23, no. 3, pp. 1318-1334, Jun. 2016.
[12] E. Davoodi, K. Zare, and E. Babaei, "A GSO-based algorithm for combined heat and power dispatch problem with modified scrounger and ranger operators," *Applied Thermal Engineering*, vol. 120, no. 25, pp. 36-48, Jun. 2017.
[13] C. Chiang, "An optimal economic dispatch algorithm for large scale power systems with cogeneration units," *European Journal of Engineering Research and Science*, vol. 1, no. 5, pp. 10-16, Nov. 2016.
[14] J. Li, J. Fang, Q. Zeng, *et al.*, "Optimal operation of the integrated electrical and heating systems to accommodate the intermittent renewable sources," *Applied Energy*, vol. 167, no. 1, pp. 244-254, Apr. 2016.
[15] X. Xu, H. Jia, H. Chiang *et al.*, "Dynamic modeling and interaction of hybrid natural gas and electricity supply system in microgrid," *IEEE Transactions on Power Systems*, vol. 30, no. 3, pp. 1212-1221, May 2015.
[16] Y. Wang, S. Wang, and L. Wu, "Distributed optimization approaches for emerging power systems operation: a review," *Electric Power Systems Research*, vol. 144, pp. 127-135, Mar. 2017.
[17] Z. Li and M. Shahidehpour, "Privacy-preserving collaborative operation of networked microgrids with the local utility grid based on enhanced benders decomposition," *IEEE Transactions on Smart Grid*, vol. 11, no. 3, pp. 2638-2651, May 2020.
[18] Z. Pan, Q. Guo, and H. Sun, "Feasible region method based integrated heat and electricity dispatch considering building thermal inertia," *Ap-*

plied Energy, vol. 192, no. 15, pp. 395-407, Apr. 2017.
[19] G. Li, Z. Bie, Y. Kou *et al.*, "Reliability evaluation of integrated energy systems based on smart agent communication," *Applied Energy*, vol. 167, no. 1, pp. 397-406, Apr. 2016.
[20] X. Lai, L. Xie, Q. Xia *et al*., "Decentralized multi-area economic dispatch via dynamic multiplier-based Lagrangian relaxation," *IEEE Transactions on Power Systems*, vol. 30, no. 6, pp. 3225-3233, Dec. 2014.
[21] X. Lai, H. Zhong, Q. Xia *et al*., "Decentralized intraday generation scheduling for multiarea power systems via dynamic multiplier-based Lagrangian relaxation," *IEEE Transactions on Power Systems*, vol. 32, no. 1, pp. 454-463, May 2016.
[22] R. Glowinski, S. Osher, and W. Yin, "Decentralized learning for wireless communications and networking," in *Splitting Methods in Communication, Imaging, Science, and Engineering*, Berlin: Springer, 2017, pp. 461.
[23] H. Zhang, Y. Li, W. Gao *et al*., "Distributed optimal energy management for energy internet," *IEEE Transactions on Industrial Informatics*, vol. 13, no. 6, pp. 3081-3097, Dec. 2017.
[24] W. Zhong, K. Xie, Y. Liu, *et al*., "ADMM empowered distributed computational intelligence for internet of energy," *IEEE Computational Intelligence Magazine*, vol. 14, no. 4, pp. 42-51, Nov. 2019.
[25] J. Chen, Z. Lin, J. Ren *et al*., "Distributed multi-scenario optimal sizing of integrated electricity and gas system based on ADMM," *International Journal of Electrical Power & Energy Systems*, vol. 117, pp. 1-10, May 2020.
[26] X. He, Y. Zhao, and T. Huang, "Optimizing the dynamic economic dispatch problem by the distributed consensus-based ADMM approach," *IEEE Transactions on Industrial Informatics*, vol. 16, no. 5, pp. 3210-3221, May 2020.
[27] ISO Department of Market Analysis and Development, Folsom, California. (2012, Feb.). Market disruption report January 16, 2012 to February 15, 2012. [Online]. Available: http://www.caiso.com/Documents/MarketDisruptionReport Nov16-Dec15_2012.pdf
[28] J. Guo, G. Hug, and O. Tonguz, "Impact of communication delay on asynchronous distributed optimal power flow using ADMM," in *Proceedings of* 2017 *IEEE International Conference on Smart Grid Communications*, Dresden, Germany, Oct. 2017, pp. 177-182.
[29] Y. Li, H, Zhang, X. Liang *et al*., "Event-triggered-based distributed cooperative energy management for multienergy systems," *IEEE Transactions on Industrial Informatics*, vol. 15, no. 4, pp. 2008-2022, Apr. 2019.
[30] L. Majzoobi, F. Lahouti, and V. Shah-Mansouri, "Analysis of distributed ADMM algorithm for consensus optimization in presence of node error," *IEEE Transactions on Signal Processing*, vol. 67, no. 7, pp. 1774-1784, Jan. 2019.
[31] L. Majzoobi, V. Shah-Mansouri, and F. Lahouti, "Analysis of distributed ADMM algorithm for consensus optimisation over lossy networks," *Institution of Engineering and Technology*, vol. 12, no. 6, pp. 786-794, Aug. 2018.
[32] J. Maurer, C. Elsner, S. Krebs *et al*., "Combined optimization of district heating and electric power networks," *Energy Procedia*, vol.149, pp. 509-518, Sept. 2018.
[33] A. Benonysson, "Dynamic modelling and operational optimization of district heating systems," Ph. D. dissertation, Laboratory of Heating and Air Conditioning, Technical University of Denmark, Lyngby, Denmark, 1991.
[34] D. Davis and W. Yin W, "Faster convergence rates of relaxed Peaceman-Rachford and ADMM under regularity assumptions," *Mathematics of Operations Research*, vol. 42, no. 3, pp. 783-805, Feb. 2017.
[35] N. Bastianello, R. Carli, L. Schenato *et al.*, "Distributed optimization over lossy networks via relaxed Peaceman-Rachford splitting: a robust ADMM approach," in *Proceedings of 2018 European Control Conference*, Limassol, Cyprus, Jun. 2018, pp. 477-482.
[36] Illinois Institute of Technology. (2020, Mar.). Test data for combined heat and power dispatch. [online]. Available: http://motor.ece.iit.edu/data
[37] J. Huang, Z. Li, and Q. Wu, "Coordinated dispatch of electric power and district heating networks: a decentralized solution using optimality condition decomposition," *Applied Energy*, vol. 206, no.15, pp. 1508-1522, Nov. 2017.
[38] C. Lin, W. Wu, B. Zhang *et al*., "Decentralized solution for combined heat and power dispatch through Benders decomposition," *IEEE Transactions on Sustainable Energy*, vol. 8, no. 4, pp. 1361-1372, Mar. 2017.

Xinyu Liang received the B. E. degree from the Department of Electrical Engineering, Nanjing Agricultural University, Nanjing, China, in 2018. She is currently working toward the M.E. degree at the School of Electric Power Engineering, South China University of Technology, Guangzhou, China. Her research interest is integrated energy system optimization.

Zhigang Li received the B. S. and Ph. D. degrees in electrical engineering from Tsinghua University, Beijing, China, in 2011 and 2016, respectively. He is currently an Associate Professor with the School of Electric Power Engineering, South China University of Technology, Guangzhou, China. He was a Visiting Scholar with the Illinois Institute of Technology, Chicago, USA, and the Argonne National Laboratory, Argonne, USA. His research interests include power system optimization, integrated energy systems analysis, and renewable energy integration.

Wenjing Huang received the B.E. degree from the School of Electric Power Engineering, South China University of Technology, Guangzhou, China, in 2019. He is currently working toward the M.E. degree in the same department. His research interest is the dispatchable region of the integrated energy system.

Q. H. Wu received an M. Sc. (Eng.) degree in electrical engineering from Huazhong University of Science and Technology, Wuhan, China, in 1981. From 1981 to 1984, he was appointed Lecturer in electrical engineering in the same university. He received a Ph. D. degree in electrical engineering from The Queen's University of Belfast (QUB), Belfast, UK, in 1987. He worked as a Research Fellow and subsequently a Senior Research Fellow in QUB from 1987 to 1991. He joined the Department of Mathematical Sciences, Loughborough University, Loughborough, UK, in 1991, as a Lecturer, and subsequently was appointed Senior Lecturer. In September 1995, he joined The University of Liverpool, Liverpool, UK, to take up his appointment to the Chair of Electrical Engineering in the Department of Electrical Engineering and Electronics. Now he is with the School of Electric Power Engineering, South China University of Technology, Guangzhou, China, as a Distinguished Professor and the Director of Energy Research Institute of the University. He has authored and coauthored more than 440 technical publications, including 220 journal papers, 20 book chapters and 3 research monographs published by Springer. He is a Fellow of IEEE, Fellow of IET, Chartered Engineer and Fellow of InstMC. His research interests include nonlinear adaptive control, mathematical morphology, evolutionary computation, power quality and power system control and operation.

Haibo Zhang received the Ph.D. degree from the Department of Electrical Engineering, Tsinghua University, Beijing, China, in 2005. He is currently a Professor with North China Electric Power University, Beijing, China. His research interests include energy management systems and power system simulation and control.